ATLAS NOTE

June 2, 2014

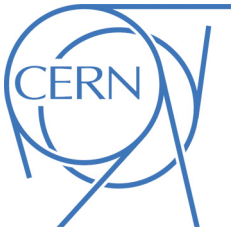

An Algorithm for Micromegas Segment Reconstruction in the Level-1 Trigger of the New Small Wheel

Brian Clark[a], David Lopez Mateos[a], Nathan Felt[a], John Huth[a], John Oliver[a]

[a]*Harvard University*

ATL-UPGRADE-INT-2014-001
03 September 2014

Abstract

This note describes the design of an algorithm for segment reconstruction in the micromegas detector of the New Small Wheel, which is part of the Phase 1 ATLAS upgrade. The algorithm performance is evaluated using a realistic geometry and digitization implemented in ATHENA. The algorithm timing, critical for operation within tight latency constraints of the level-1 trigger, is evaluated using a digital simulation of an FPGA. Segment building is performed in at most 38 ns in addition to a integration time maximum of two bunch crossings (50 ns), with high efficiency and rejection of tested incoherent and coherent backgrounds.

1 Introduction

The trigger system for the endcap muon detectors in ATLAS currently relies on the use of the middle layer (EM) and the reconstruction of projective segments pointing to the interaction point (IP) by the thin-gap chambers (TGCs) [1]. During Run 1, increased trigger rates were observed due to secondary particles that formed in material near the beampipe outside the endcap toroid. The new small wheel [**?**] (NSW) will provide robustness in the trigger by generating track segments for the level-1 trigger. The micromegas trigger processor must provide reconstructed segments to the level-1 trigger logic to be combined with segments identified in the sTGC detectors of the NSW and later used in conjunction with segments constructed in the EM chambers. These segments should project in θ back to the IP within some reasonable tolerance (roughly 10 mrad). The deviation from projectivity, $\Delta\theta$, needs to also be reported to aid in the level-1 muon momentum reconstruction. In addition to $\Delta\theta$, the trigger processor must also provide a Region of Interest (ROI) in both azimuth and pseudorapdity to allow for accurate segment association between the NSW segments and the segments reconstructed in the EM chambers.

The purpose of this note is to develop and study the performance of a trigger algorithm for the micromegas. This note is organized as follows. Section 3 describes in detail the segment-building algorithm. Section 4 describes the digital simulation used to understand the performance of the algorithm in the FPGA and the algorithm timing obtained from that simulation. Section 5 describes the Monte Carlo simulation and background model used for performance studies. Section 6 describes the choice of tunable parameters in the algorithm. Section 7 evaluates the performance of the algorithm. Section 8 describes some additional studies on coherent backgrounds and Section 9 offers some concluding remarks.

2 Detector Geometry

Figure 1 illustrates some of the relevant features of this geometry. In this figure, and the rest of the note, the ATLAS coordinate system is used, a right-handed coordinate system with the z direction along the beam pipe and origin at the center of the detector. Figure 1(a) illustrates the view of one NSW sector on the xy-plane, perpendicular to the beam, with the beam pipe below the wedge and exaggerating the tilt of the U and V strips. Figure 1(b) shows the layout of the readout planes along the z direction with the IP to the left. The z positions of each readout plane are also specified. For the studies in this note, three horizontal detector gaps of 10 mm exist in the wedge as a wedge was originally expected to be composed of four modules at different radial distances from the beam line. This geometry differs from the last NSW design, which consists only of two modules, and thus contains only 1 gap. This modular geometry is also illustrated in Figure 1 (a).

3 Algorithm Description

The trigger algorithm is illustrated in Figures 2 and 3. The alphabetical labeling in Figure 2 corresponds to the proceeding bullet points detailing various algorithm operations.

(A) Incoming strip hit addresses are converted to slope values using a look-up table. A strip's stored slope value is defined as the orthogonal distance between a given strip and the beam line divided by the z location of the relevant detection plane.

(B) Hit slope values are stored in a circular buffer defined as (N slope-roads) $\times$ (8 planes) $\times$ (T), where T is the cyclical buffer depth. A track candidate is identified once a minimum hit threshold is met.[1]

[1] More precisely, there are two circular buffers working in unison. One buffer stores strip number and slope information, while the other buffer stores binary markers indicating the presence of a hit. The latter is used for triggering a coincidence threshold, while the former is readout for track fitting once a threshold has been met.

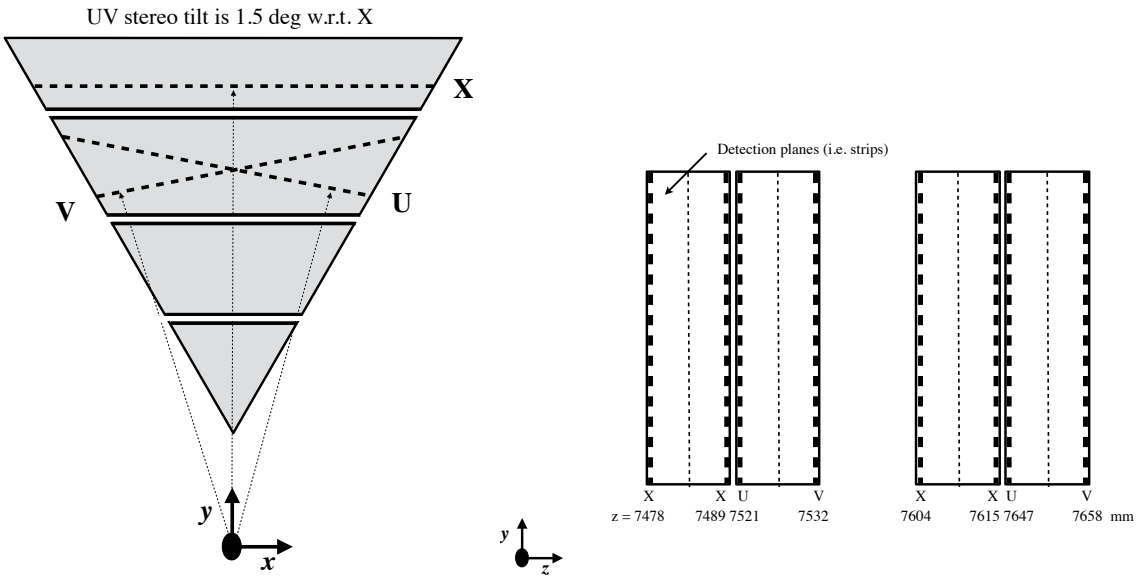

(a) (b)

Figure 1: (a) As shown in the *xy*-plane, stereo planes are defined by X (0 deg), U (1.5 deg), and V (−1.5 deg) detection strips, where a single detection plane has one type of strip orientation. (b) Eight planes form one wedge with XXUVXXUV layout. The drift gaps between detection planes for charge deposition and amplification are approximately 5 mm.

Key points defining the buffer operation:

a) Unless explicitly stated otherwise, $T = 2$ for studies in this note, which corresponds to two bunch crossings. The buffer advances every bunch crossing (25 ns). A 50 ns maximum lifetime for hits to form coincidence within a slope-road was chosen given the high number of first-arrival hits that present well within 50 ns of muon-detector interaction (i.e. drift times are generally <50 ns).

b) The solid angle covered by one wedge is divided into N "slope-roads." (See Figure 4. N is determined by the minimum and maximum allowed slopes, which are geometric constraints of the NSW, and the size of the slope-roads, parameterized by an incremental slope value, h. Details on the optimization of the value of h can be found in Section 6.

c) The size of a slope-road was chosen to be 2.5×10^{-4} (Section 6). This corresponds to approximately 4 strips on the innermost large wedge detection plane.

d) An X hit will be recorded in its respective slope-road (first buffer index) and detection plane (second buffer index). To reduce the effect of static slope-road boundaries, a tolerance factor is applied corresponding to slope±0.5×h; this implies that the hit will also be recorded in the next closest slope-road. This is illustrated in Figure 5.

e) A U(V) hit will be recorded in the slope-road that corresponds to its calculated slope. Due to the 1.5 deg tilt of stereo plane strips, a larger tolerance factor is applied corresponding to slope±0.0035 (Section 6), which is approximately slope-road ±14 slope-roads. This is again illustrated in Figure 5.

(C) Each slope-road of the buffer is checked once per bunch crossing to determine if a coincidence threshold has been met, where coincidence independently requires a minimum number of X and UV planes to be hit in a given slope-road and the oldest piece of data be timing out (i.e., one entry

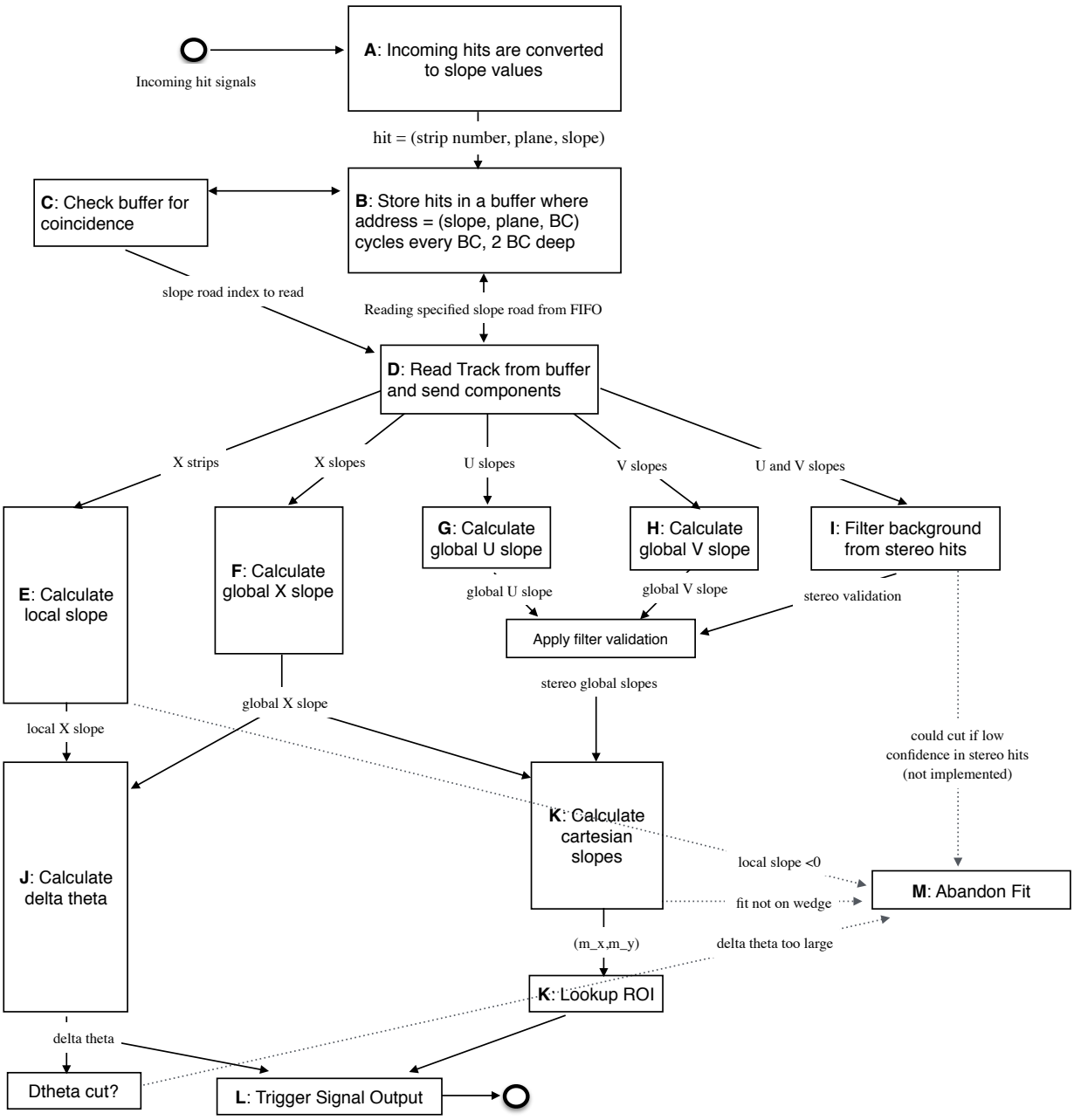

Figure 2: The block diagram is constructed with time flowing downward; therefore tasks on the same horizontal line are accomplished in parallel. Blocks correspond to operations comprising the algorithm, solid flow lines represent the flow of data, and light dotted lines represent fit abandonment signals, which can be triggered at multiple points throughout the algorithm. Blocks after step D are approximately sized to represent their relative processing times.

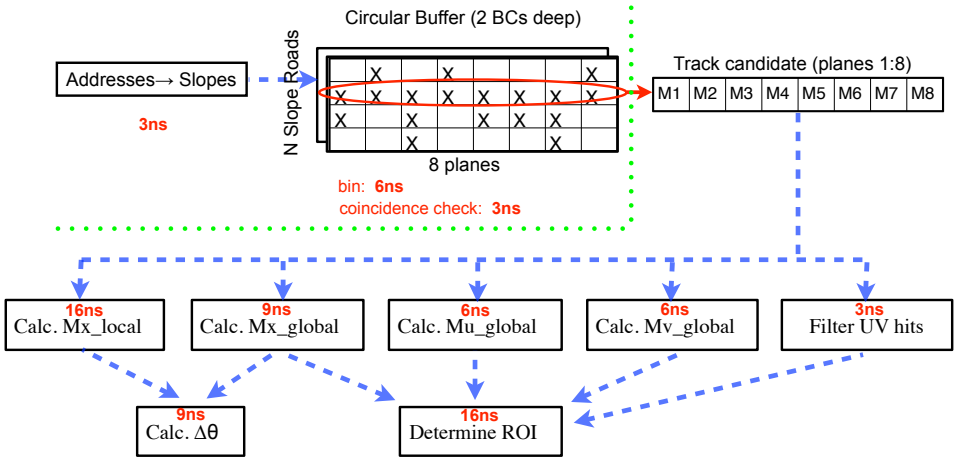

Figure 3: This figure provides another visualization of the algorithm. Specifically, the function of the circular buffer is represented as a coincidence filter.

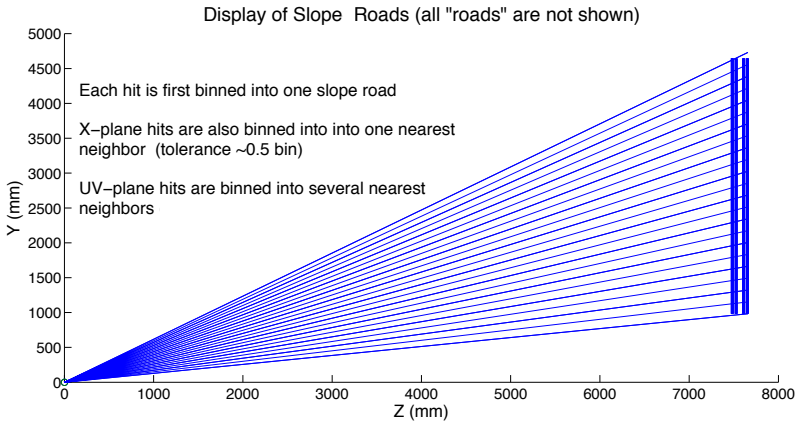

Figure 4: The detection region for a wedge is divided into many static slope-roads anchored to the IP.

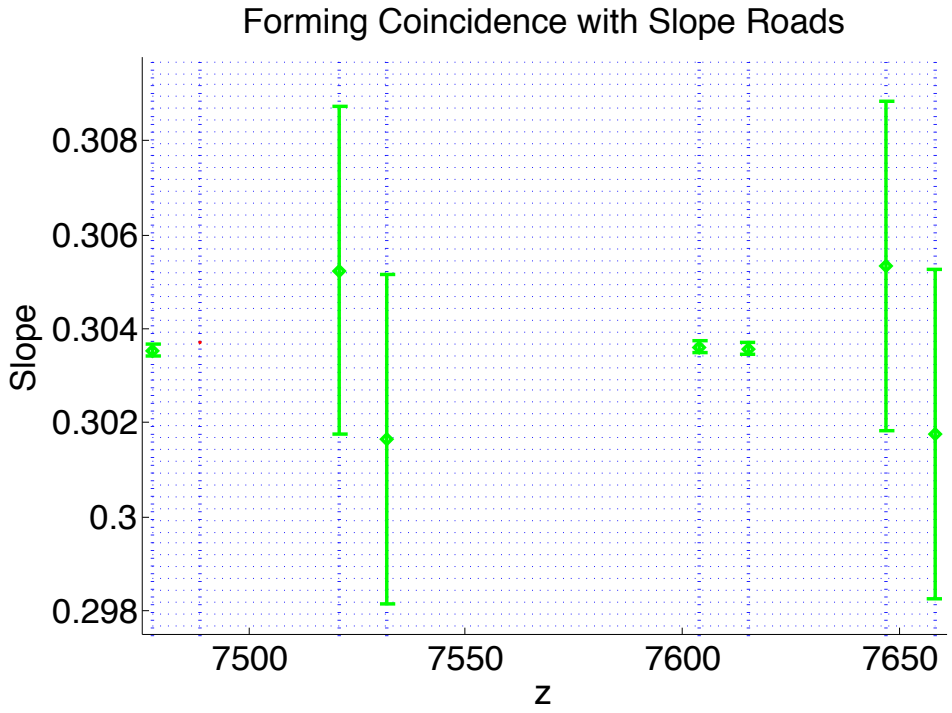

(a)

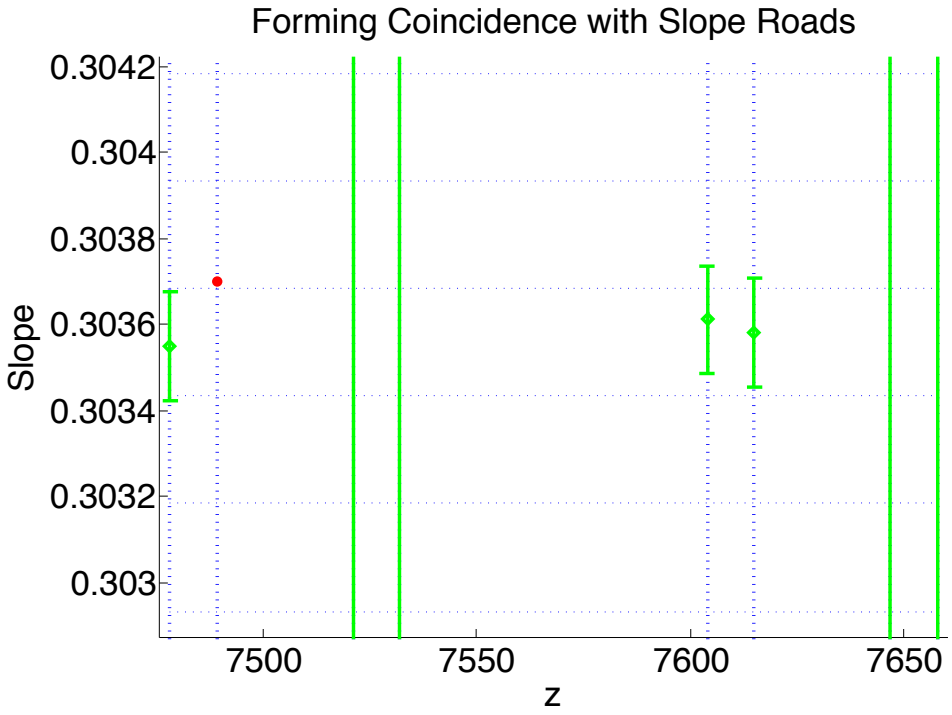

(b)

Figure 5: This figure visualizes coincidence formation for a true event. Green indicates a hit that was included in the fit. Red indicates a hit that was not included due to its arrival after 50 ns, where time zero is the first energy deposited in the first plane of the detector. Vertical dashed blue lines are the planes (XXUVXXUV). Horizontal dotted blue lines are the slope-road boundaries. Error bars on green hits represent tolerance for forming coincidence. As seen in (a), tolerance is greater for U and V planes than for X planes. Zooming in on the hits (b), we see that X tolerance implies that each hit spans 2 slope-roads. In this event, the slope-road containing slope=0.3036 was readout because it satisfied a coincidence threshold that was set to 2X+2UV hits. The slope-road directly above also satisfied this threshold, but the road most exceeding a threshold will be chosen among adjacent slope-roads.

in the proposed track is older than one bunch crossing). Coincidence identification is accomplished using the binary hit configuration for a given slope-road as the address of a lookup table that is pre-populated with pass or no-pass signals for various hit configurations eight planes. Rather than searching the entire buffer for hits, only active areas are interrogated for confidence verification.[2]

The choice of specific values of tunable parameters – including slope-road size, UV slope tolerance, coincidence window T, the necessary number of X and UV hits for coincidence – is addressed in Section 6.

(D) slope-road contents containing the track candidate are read and cleared from the buffer and relevant track components are forwarded for processing.

Once a candidate track is identified, the following steps (E-I) are completed in parallel:

(E) A local slope is calculated using a least squares fit of available X hits in the proposed track. The local slope fit is reasonably quick (5 clock ticks, or $\approx$ 16ns for a 320 MHz clock) as many constants are stored in a look-up table for the 11 possible combinations (indexed by $k = \{1..11\}$) of $n = \{2, 3, 4\}$ X hits.

$$M_X^{local} = A_k \sum_{i=1}^{n} z_i y_i - B_k \sum_{i=1}^{n} y_i \tag{1}$$

where

$$A_k = \frac{n}{n \sum_{i=1}^{n} z_i^2 - (\sum_{i=1}^{n} z_i)^2} \tag{2a}$$

$$B_k = \frac{\sum_{i=1}^{n} z_i}{n \sum_{i=1}^{n} z_i^2 - (\sum_{i=1}^{n} z_i)^2} \tag{2b}$$

(F) A global X hit slope, M_X^{global}, which is anchored to the IP, is calculated as the average of registered $n = \{2, 3, 4\}$ X hits in the proposed track candidate. Note, $n = 1$ is not allowed because requiring a non-trivial local slope places places a minimum of two X hits.

$$M_X^{global} = \frac{\sum_{i=1}^{n} (M_X)_i}{n} \tag{3}$$

(G) A global U hit slope, M_U^{global}, which is anchored to the IP, is calculated as the average of registered $n = \{1, 2\}$ U hits in the proposed track candidate.

$$M_U^{global} = \frac{\sum_{i=1}^{n} (M_U)_i}{n} \tag{4}$$

[2]The algorithm described in this paper uses a large memory bank as a circular buffer for forming coincidence. Our firmware version operates under the same principles, but with a modified implementation to efficiently make use of FPGA resources.

(H) A global V hit slope, M_V^{global}, which is anchored to the IP, is calculated as the average of registered $n = \{1, 2\}$ V hits in the proposed track candidate.

$$M_V^{global} = \frac{\sum_{i=1}^{n} (M_V)_i}{n} \tag{5}$$

(I) As previously mentioned, the "slope-road tolerance" for forming coincidence with U/V hits is many strips large. This large tolerance in comparison to ionization spread increases the likelihood of a background hit corrupting the proposed track. U/V background hits are further filtered from proposed tracks by judging how correlated two U/V hits are with one another. The logic outline is the following:

(a) Given two U or V hits, are their slopes equal within a tolerance factor? (The tolerance factor was not independently optimized in these studies, but was taken to be the size of a slope-road, h.) Specifically,

i) is $|(M_U)_1 - (M_U)_2| < h$?

ii) is $|(M_V)_1 - (M_V)_2| < h$?

iii) The absence of a second U(V) hit implies the above criterion $i(ii)$ is not met for purposes of the filtering logic below.

(b) The filtering logic then considers the following:

i) If both pairs of U and V hits are sufficiently correlated (i.e. present as "true" from logic above), then both pairs of hits are kept.

ii) If only one pair of U or V hits is sufficiently correlated (i.e. presents as "true"), then that pair is kept and the uncorrelated stereo hits are disregarded.

iii) If both present as "false," then no filtering is applied. (An option could naturally be introduced here to abandon the fit, but we chose not to implement such an option in these studies.)

(J) $\Delta\theta$ is calculated using previously fitted M_X^{global} and M_X^{local} values. This calculation is accomplished using

$$\Delta\theta = \frac{M_X^{local} - M_X^{global}}{sin(\phi) + \frac{M_X^{local} M_X^{global}}{sin(\phi)}} \approx \frac{M_X^{local} - M_X^{global}}{1 + M_X^{local} M_X^{global}} \tag{6}$$

where, recalling that calculated slope values are projection is the yz-plane, $sin(\phi) = 1$, and $\phi^{global} \approx \phi^{local}$. These approximation introduces $< 4\%$ error into the $\Delta\theta$ calculation. In our hardware implementation, division is a time intensive process; therefore, we have introduced a look-up table that approximates the denominator with negligible error introduced and provides additional background filtering by removing tracks with negative-value local slopes, which is indicative of track origination outside of the detector. The computation of this quantity in the FPGA proceeds as follows:

a) Calculate $M_X^{local} - M_X^{global}$.

b) Calculate $M_X^{local} M_X^{global}$.

c) Use result of step (b) to locate the reciprocal of $(1 + M_X^{local} M_X^{global})$ in a reference table.

d) Multiply the results of steps (a) and (c) to solve Equation 6

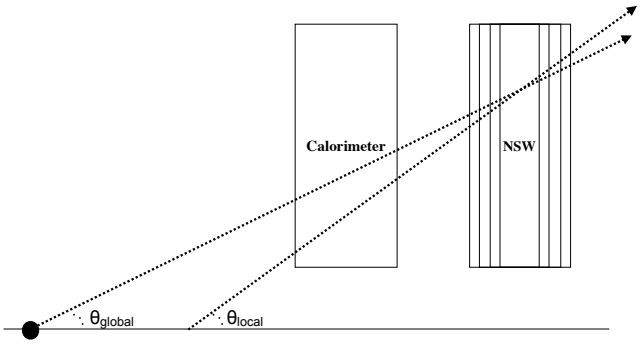

Figure 6: $\Delta\theta = \theta^{local} - \theta^{global}$, where $\theta^{global} \approx M_X^{global}$ and $\theta^{local} \approx M_X^{local}$

.

(K) A Region of Interest (ROI) is determined using previously calculated M_U^{global} and M_V^{global} values. The following steps are taken:

(a) Calculate Cartesian slope coordinates (m_x, m_y), where $m_y = M_X^{global}$ and m_x is given by:

i) if M_U^{global} and M_V^{global} are both non-zero, i.e. not filtered by (H), then

$$m_x = A(M_U^{global} - M_V^{global}) \tag{7}$$

.

ii) if only one global stereo slope remains after filtering, then

$$m_x = AM_U^{global} - BM_X^{global} \tag{8a}$$

$$m_x = -AM_V^{global} + BM_X^{global} \tag{8b}$$

where $A \equiv \csc(1.5 \text{ deg})$ and $B \equiv \cot(1.5 \text{ deg})$.

(b) Truncate (m_x, m_y) and use as the address of a look-up table that converts $(m_x, m_y) \rightarrow (\theta, \phi)$.

(L) A $\Delta\theta$ and ROI are offered as a trigger signal.

(M) There are many points in which a fit may be abandoned as the track candidate is determined to be either insufficient for an accurate fit or the product of background.

a) No coincidence is formed to meet the minimum threshold. This will happen in the case of a true track when background masks the track by timing-out the VMM chip, thereby hiding a would-be trigger hit.

b) $M_X^{local} M_X^{global} < 0$ in step (D). This would happen in the case of a negative local slope value, which is indicative of a track not originating at the origin. A negative local slope could also occur if there were only 2 X hits on adjacent planes (i.e. small lever arm for fit) and one of the hits was background.

c) (m_x, m_y) does not refer to an ROI covered by the wedge. This can happen in situations of significant background insertion into our track candidate or secondary tracks in close proximity to one another, thereby disrupting the relation between U and V if stereo hits from each track are taken; the error in this case is most notably in ϕ. Also, very high energy muons causing considerable showering in the detector present the aforementioned issues.

d) $\Delta\theta$ is not within a prescribed range of values corresponding to tracks from the region of the IP. Note, slope-roads offer an initial geometric $\Delta\theta$ cut, so this should be seen as a finer cut.

4 Algorithm timing

Timing estimates for the steps of the previous section are shown Figure 7. The trigger algorithm's longest path is ≈37 ns, assuming all necessary hits arrive promptly and track fitting begins immediately. However, the algorithm implements a 50 ns waiting period for hits to accumulate before beginning track fitting operations. Once this accumulation period expires, the algorithm requires a maximum of 9 clock tics, or ≈28 ns, to determine if a coincidence threshold has been satisfied and perform fitting operations (denoted by green line) to determine $\Delta\theta$ and the ROI. Therefore, the entire latency time is approximately three bunch crossings.[3] Timing estimates assume 1 clock tic for each addition and multiplication operations and 1 clock tic for each table lookup, where the clock frequency is 320MHz.

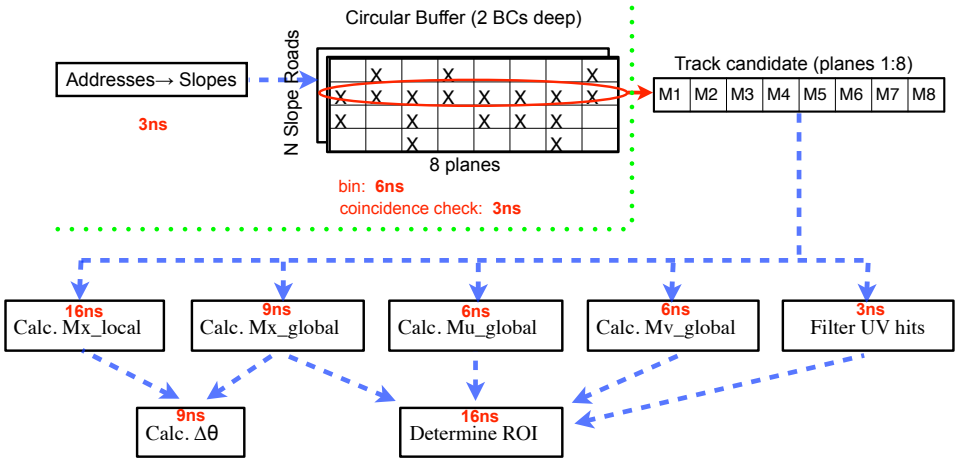

Figure 7: The longest path is ≈37 ns. The hit accumulation time window for forming coincidence is a tunable parameter to be studied in detail.

These results are confirmed by an FPGA implementation of the algorithm targeting a Xilinx Vertex 7 board with a 320MHz clock constraint and no timing errors. An image showing the timing of the FPGA implementation is shown in Figure 8.

5 Monte Carlo Simulation

5.1 Event generation

Single muon events were generated with ATHENA full simulation implementing the geometry described in Section 2 and using typical parameters of the ATLAS beamspot during Run 1 for the primary sample used in the studies. This sample was composed of muons of $E = 200$ GeV generated in the proximity of the detector center with mean (x, y, z) of $(0.05, 0.06, -1)$ mm and with a gaussian spread $(\sigma_x, \sigma_y, \sigma_z)$ of $(0.01, 0.01, 70)$ mm.

In addition, to study real muon background track rejection, a sample with muons generated at $(0, 0, 1500)$ mm and with $E = 200$ GeV was investigated. To increase statistics and focus on a single large wedge of the NSW, muons were simulated only within the solid angle defined by $\theta_{min} = 0.1722$, $\theta_{max} = 0.5254$, $\phi_{min} = 1.3028$, $\phi_{max} = 1.8388$. Of the digitized hits found in the simulation, the first registered signal per channel was chosen for trigger construction. A function mimicking a VMM chip's

[3] The 28 ns fitting time is set, however, the remaining prior steps can be included in the 50 ns hit accumulation time window.

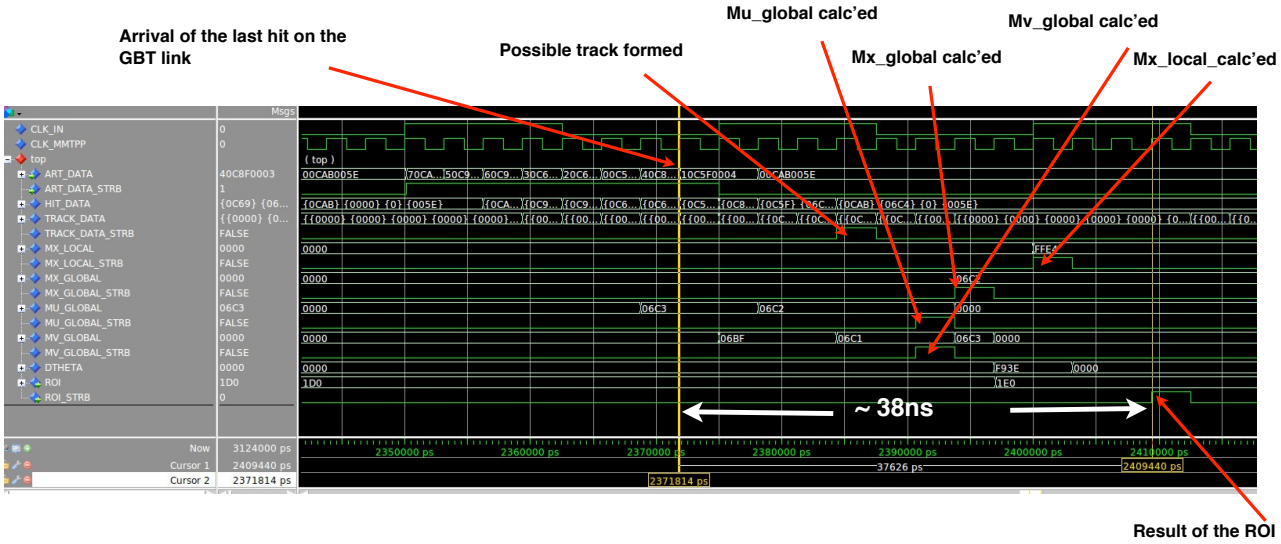

Figure 8: Timing estimates were confirmed by a hardware simulation targeting a Xilinx Vertex 7 part with a 320 MHz clock.

100 ns deadtime and coverage of 64 strips was then applied to the data. This function serves to guarantee a maximum of one hit, true or background, is registered for each 64 grouping of strips for each event.

5.2 Background Simulation

Incoherent background extrapolated from measurements performed in Run 1 [3], and characterized by Figure 9 is added outside of ATHENA to each generated event as hits after the digitization step, performed in ATHENA. Background hits are uniformly distributed in ϕ, within our aforementioned cuts, and in time across two bunch crossings (50 ns). Once generated for each event, the background hits are combined with true event hits and a VMM-mimicking function is called by the simulation to choose only the earliest arrival hit for each VMM chip, which allows for the background to sometimes mask a true trigger hit.

6 Choice of Parameter Values

There are currently four parameters that can be tuned in the trigger algorithm: slope-road size, UV tolerance, coincidence threshold, and coincidence gathering time window. Subsets of ≈2000 events from our larger data samples were used for parameter tuning purposes.

6.1 Coincidence Threshold

Coincidence for these studies were purposefully chosen to be minimal requiring 2X+2UV. This requirement is the lowest threshold setting that allows independent coincidence determination in X and UV planes. This low setting also offers the poorest resolution in track reconstruction. However, it will be shown in the results below that the previous slope-road tuning sufficiently limits background influence such that efficiency and resolution are quite good. Increasing the threshold will decrease the number of candidate events while also improving resolution in $\theta, \phi, \Delta\theta$.

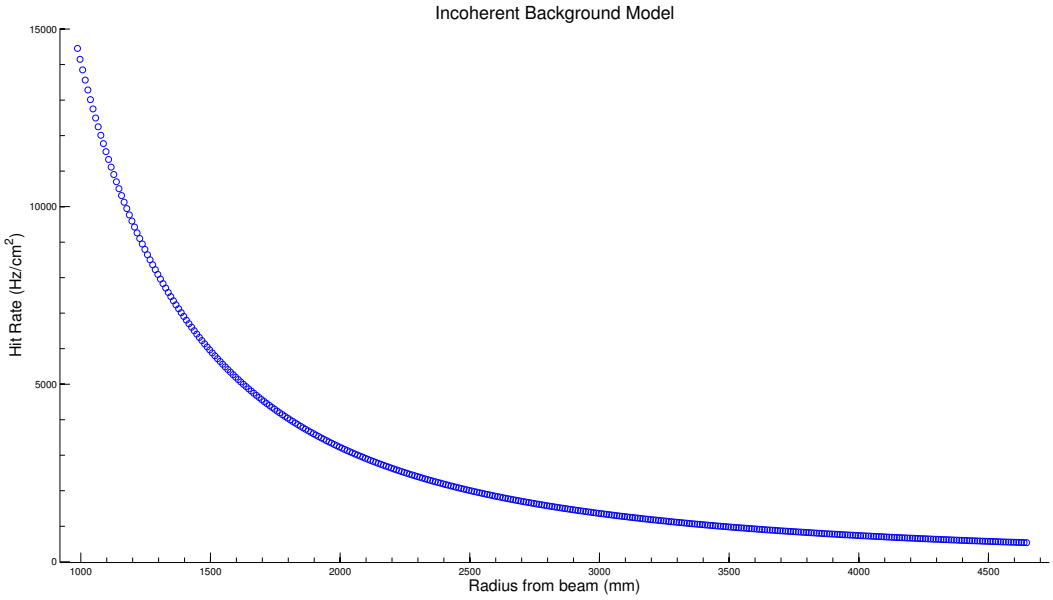

Figure 9: Incoherent background hit rate as a function of the radial distance from the beam line. The background is estimated following extrapolations based on data recorded during Run 1 and reported in Ref. [3].

6.2 Charge Threshold and Coincidence Formation Time

The coincidence formation time was taken to be 50 ns, which corresponds to two bunch crossings. All charge is collected within 100 ns, but most drift times for first-arrival-hits, which are used for triggering, are less than 50 ns. Therefore, shrinking the coincidence window from 100 ns to 50 ns changes the fit efficiency very little.

Charge thresholds to register a trigger strip hit were set at approximately $10^5 e$. This value is a benchmark that developers of the VMM chip currently believe might be the best achievable. Additional studies, showing the change in performance as this value is changed are beyond the scope of this note.

6.3 Tuning Slope-road Size

Events were fitted with a coincidence requirement of at least 2 X hits and no minimum number of UV hits. Figure 10 shows the number of fitted events as a function of the slope-road size. Not shown on the graph to the left is a steep decrease in fit efficiency as h becomes smaller than the size of a strip width. Efficiency declines as h increases due to the increased likelihood and impact of background entering the track fit. The optimal slope-road size was chosen to be 2.5×10^{-4}. This slope-road size corresponds to approximately 4 strip widths on the innermost detector plane. This tuning is dependent upon the coincidence threshold chosen for X hits. If the coincidence threshold is increased, then the optimal slope-road size will increase slightly.

6.4 Tuning UV Tolerance

Events were fitted with a coincidence requirement of at least 2 X hits and 2 UV hits. Recall that UV hits are given a larger tolerance filling several slope-roads. In this case, the X-strip slope-road size was

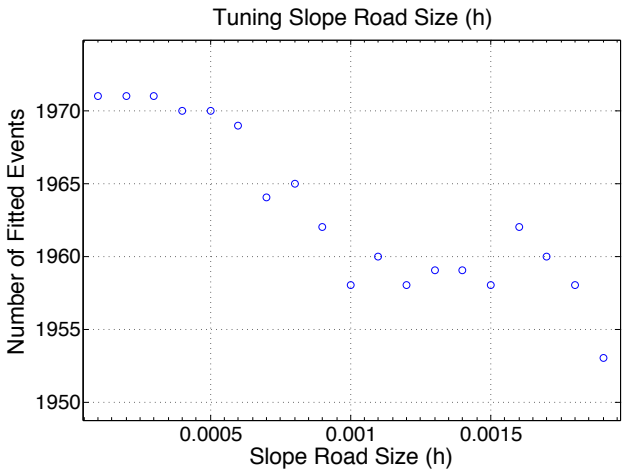

Figure 10: Number of fitted events in the tuning sample with incoherent background as a function of X-strip slope-road size.

chosen to be the optimized value, $h = 2.5 \times 10^{-4}$. Figure 11 shows the number of fitted events (blue markers) and the number of fitted events with at least a background hit (green markers) as a function of UV-strip slope-road size. The fit efficiency increases rapidly as UV tolerance approaches $\approx 3\times10^{-3}$, then drops off as as UV tolerance continues to increase. The rise in efficiency is due an increased inclusion of tracks as we include the average hit spread due to ionization and track inclination. The decrease in efficiency corresponds to the increased likelihood of The incoherent background hits disrupting a fit. As supported by this study, the optimal slope-road size was chosen to be 3.5×10^{-3}, which corresponds to $\approx$14 slope-roads.

7 Algorithm Performance

The proposed trigger algorithm was tested on an ATHENA-generated data sample of approximately 20,000 single muon events from the IP with energy 200 GeV. Digitized hits were assigned a strip address in the NSW and VMM-chip dead time was applied. When referenced, "with background" refers to the inclusion of realistic incoherent background before the VMM-chip dead time was imposed. The coincidence threshold was 2X + 2UV hits in a given slope-road, where 2UV simply implies any combination of 2 stereo hits. The window for hit accumulation was set to 50ns.

The efficiency and intrinsic resolution of the algorithm under these constraints is given without background, Table 1, and with background, Table 2. Intrinsic resolution values are presented as a standard deviation of a gaussian fit of error values. Error values are defined as $\theta^{\text{fit}}-\theta^{\text{true}}$, $\phi^{\text{fit}}-\phi^{\text{true}}$, and $\Delta\theta^{\text{fit}}-\Delta\theta^{\text{true}}$. Truth values are ATHENA truth values at the entrance of the NSW (Figure 12). "Fit Efficiency" refers to the efficiency for a track to trigger the detector. This efficiency is calculated as the number of events fitted divided by the total number of qualified events in the data sample, where "qualified" refers events with a minimum number of hits without background inclusion. "(2X+2UV)" refers to the data sample (15156 events) interrogated having at least 2X and 2UV planes hit before background was added to the event. Similarly, "(3X+3UV)" refers to the data sample (14252 events) interrogated having at least 3X and 3UV planes hit before background was added to the event. Finally, "(4X+4UV)" have exactly one hit per plane (13240 events). The three different data subsets were chosen to show how fit resolution increases with the increased number of hits registered by the detector.

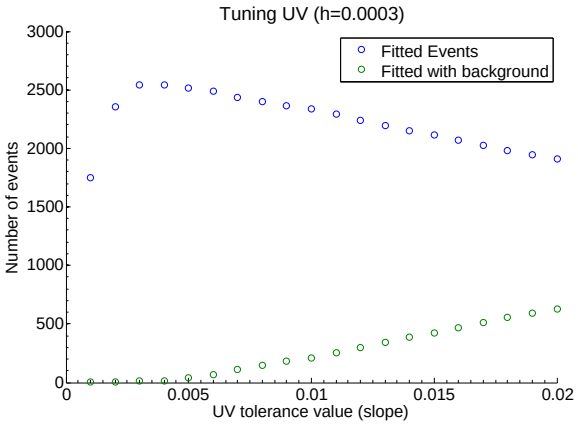

Figure 11: Number of fitted events in the tuning sample with incoherent background as a function of UV-strip tolerance (blue markers) and number of events with at least a background hit entering the fit (green markers).

Gaussian fits are calculated with a one step recursive fit. The raw results are first fitted to a gaussian. "Tails" are defined as the percent of events outside a 3σ core of this raw data fit. The tails are removed, which most consists of outliers, and the remaining data is fitted to a gaussian distribution to determine fit resolution.

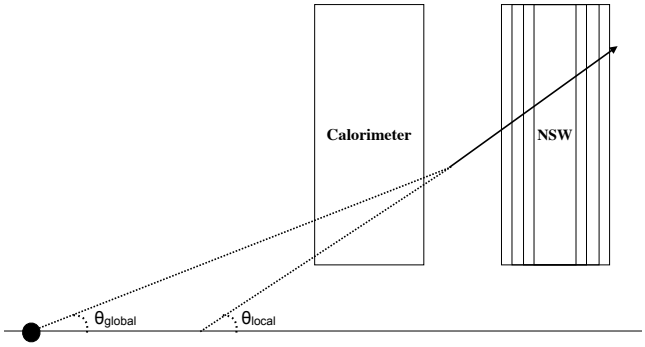

Figure 12: Truth values are taken just before entering the NSW when quantifying intrinsic resolution.

Table 1: Efficiency and resolution (mrad) for different coincidence thresholds without background.

Track Type	Fit Efficiency	$\sigma(\theta_{error})$ (tails)	$\sigma(\phi_{error})$ (tails)	$\sigma(\Delta\theta_{error})$ (tails)
(4X+4UV)	100.0%	0.27 (0.83%)	2.5 (1.5%)	1.5 (0.65%)
(3X+3UV)	99.8%	0.28 (0.89%)	3.0 (0.97%)	1.7 (0.47%)
(2X+2UV)	99.8%	0.29 (0.97%)	3.2 (1.1%)	1.9 (1.0%)

Table 2: Efficiency and resolution (mrad) for different coincidence thresholds with background.

Track Type	Fit Efficiency	$\sigma(\theta_{error})$ (tails)	$\sigma(\phi_{error})$ (tails)	$\sigma(\Delta\theta_{error})$ (tails)
(4X+4UV)	99.5%	0.30 (1.4%)	4.2 (1.5%)	1.7 (0.37%)
(3X+3UV)	99.3%	0.31 (1.9%)	4.8 (2.1%)	2.0 (0.58%)
(2X+2UV)	99.0%	0.32 (2.0%)	5.1 (2.2%)	2.3 (0.82%)

8 Background Rejection

In our incoherent background model, background hits rarely constitute a significant number of fitted hits in a track (Figure 13). This is due to the incoherent nature of our background. However, it should be noted that background tracks originating sufficiently far from the IP will appear incoherent when slope-roads are superimposed with origins at the at the center of the detector. In this way, slope-roads offer a geometric cut on background, which saves valuable computation time in the fitting algorithm.

To provide an initial study of tracks originating far from the center of the detector, we generated a data set of 11264 tracks originating near z = 1.5 m (Figure 14) and entering the NSW. With coincidence

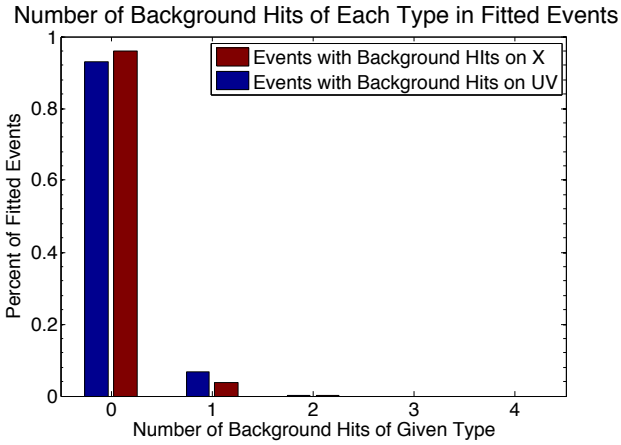

Figure 13: With coincidence thresholds set at 2X+2UV, background rarely corrupted our track fits.

thresholds set at 2 X and 2UV, 0.7% of the "background" tracks were triggered. This background triggering is expected to decrease as we move further from the center of the detector, however, additional studies will be needed to confirm this statement.

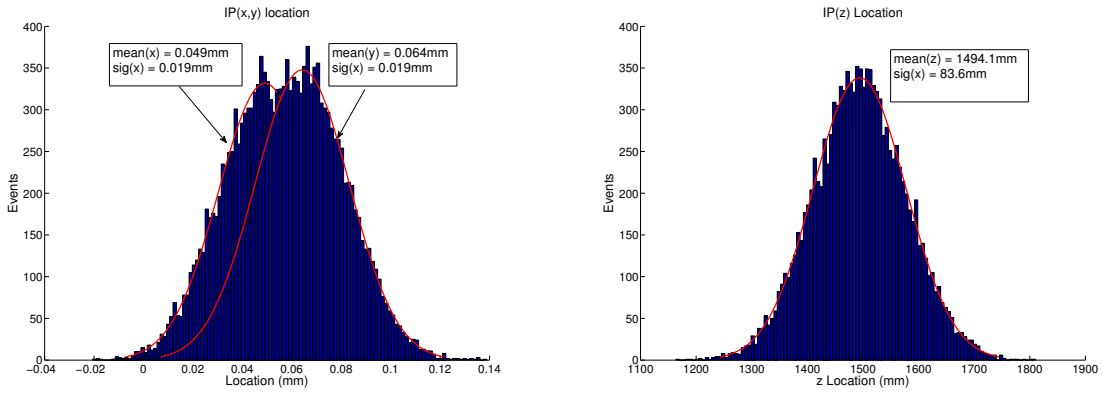

(a) (b)

Figure 14: Notice that the IP spread is displaced to $z = 1500$ mm. This shift was used to conduct an initial study of how the trigger algorithm reacts to a coherent source of background.

9 Conclusion

This note has described an algorithm for forming segments in the Micromegas New Small Wheel trigger processor. The algorithm provides an ROI for the found segments and a measure of the deviation from projectivity with a spread of about 2 mrad in the presence of incoherent background hits. The efficiency of the algorithm is above 99% for muons for which enough hits exist in the detector. The algorithm implements a tunable 50 ns waiting time to collect the vast majority of detector hits, which take some time to reach the read-out electronics due to ionization statistics and drift time. After that waiting time, the algorithm produces an output that can be sent to the sector logic within 28 ns, well within the required

allocated latency of the system.

References

[1] ATLAS Collaboration, G. Aad et al., JINST **3** (2008) S08003.

[2] T. Kawamoto et al., Tech. Rep. CERN-LHCC-2013-006. ATLAS-TDR-020, CERN, Geneva, Jun, 2013.

[3] ATLAS Collaboration, Tech. Rep. CERN-LHCC-2011-012. LHCC-I-020, CERN, Geneva, Nov, 2011.